2017

DHX33 transcriptionally controls genes involved in the cell cycle

Baolel Yuan
Southern University of Science and Technology, Shenzhen

Xingshun Wang
Southern University of Science and Technology, Shenzhen

Chunyan Fan
Southern University of Science and Technology, Shenzhen

Jin You
Southern University of Science and Technology, Shenzhen

Yuchu Liu
Southern University of Science and Technology, Shenzhen

See next page for additional authors

AMERICAN SOCIETY FOR MICROBIOLOGY | Molecular and Cellular Biology

DHX33 Transcriptionally Controls Genes Involved in the Cell Cycle

Baolei Yuan,[a] Xingshun Wang,[a] Chunyan Fan,[a] Jin You,[a] Yuchu Liu,[a] Jason D. Weber,[b] Hanbing Zhong,[a] Yandong Zhang[a]

Department of Biology, Southern University of Science and Technology, Shenzhen, China[a]; ICCE Institute, Department of Internal Medicine, Division of Molecular Oncology, Washington University School of Medicine, Saint Louis, Missouri, USA[b]

The RNA helicase DHX33 has been shown to be a critical regulator of cell proliferation and growth. However, the underlying mechanisms behind DHX33 function remain incompletely understood. We present original evidence in multiple cell lines that DHX33 transcriptionally controls the expression of genes involved in the cell cycle, notably cyclin, E2F1, cell division cycle (CDC), and minichromosome maintenance (MCM) genes. DHX33 physically associates with the promoters of these genes and controls the loading of active RNA polymerase II onto these promoters. DHX33 deficiency abrogates cell cycle progression and DNA replication and leads to cell apoptosis. In zebrafish, CRISPR-mediated knockout of DHX33 results in downregulation of cyclin A2, cyclin B2, cyclin D1, cyclin E2, cdc6, cdc20, E2F1, and MCM complexes in DHX33 knockout embryos. Additionally, we found the overexpression of DHX33 in a subset of non-small-cell lung cancers and in Ras-mutated human lung cancer cell lines. Forced reduction of DHX33 in these cancer cells abolished tumor formation *in vivo*. Our study demonstrates for the first time that DHX33 acts as a direct transcriptional regulator to promote cell cycle progression and plays an important role in driving cell proliferation during both embryo development and tumorigenesis.

DHX33 belongs to a family of DEAD/DEAH box RNA helicases, characterized by multiple conserved peptide motifs in their primary amino acid sequences, that are important for substrate binding and ATP hydrolysis. RNA helicases can couple ATP hydrolysis with the conformational change of RNP complexes to influence diverse activities of RNA, such as ribosome biogenesis, microRNA (miRNA) biogenesis, transcription, splicing, translation, and mRNA decay (1, 2).

In previous studies, we identified DHX33 to be a significant player in ribosome RNA synthesis and mRNA translation (3, 4). Other research groups have found DHX33 to be important in innate immunity as it can sense double-stranded RNA (dsRNA) from pathogens (5, 6). Despite this earlier work, the detailed molecular mechanisms of how DHX33 promotes numerous cellular processes, such as cell proliferation, remain poorly defined. We have identified DHX33 as a downstream transcriptional and translational target of Ras that is sensitive to signals emanating from the phosphatidylinositol 3-kinase (PI3K)/Akt/mTOR pathway (7). As the *Ras* gene has a mutation rate of 35% in non-small-cell lung cancer (NSCLC), we sought to use established lung cancers as a model for dysregulation of endogenous DHX33 expression.

Lung cancer can be divided into two major categories: small-cell lung cancer comprising 20% and NSCLC comprising 80% of all cases (8). Comprehensive cancer genome sequencing has found both genetic and epigenetic alterations tightly correlated with non-small-cell lung cancer development (9, 10). Among these genetic alterations, mutations of cancer-critical genes have been frequently detected in NSCLC; these include epidermal growth factor receptor (EGFR), Ras, anaplastic lymphoma kinase (ALK), and p53 genes (9–12). Two prominent drug targets are ALK and EGFR, whose inhibitors have been widely used to treat patients (12, 13). A recent report showed that activation of the Ras signaling pathway accounts for more than 70% of all cases of NSCLC (9). However, no efficient therapy for Ras-mutated cancers has been developed, and it is well known that Ras protein is a notoriously difficult molecular target in the clinic (14). As such, it is important that we identify other critical targets that reside downstream of Ras.

In this report, we found that DHX33 promotes cell proliferation by transcriptionally regulating genes that control cell cycle progression. DHX33 expression is required for continued cell proliferation as it promotes cell cycle progression at the G_1/S, G_2/M, and metaphase-anaphase transitions. DHX33 physically associates with the promoters of numerous cell cycle genes where it acts to recruit active RNA polymerase II (Pol II) loading.

To confirm established cell line data, we used a zebrafish model system to study the role of DHX33 during embryo development *in vivo*. DHX33 gene knockout results in severe brain, eye, and liver developmental defects. DHX33 knockout caused downregulation of critical genes involved in cell cycle control, especially the cyclin A2, cyclin B2, cyclin D1, cyclin E2, E2F1, cdc6, cdc20, and minichromosome maintenance (MCM) complex genes.

We further used a lung cancer tissue microarray to evaluate DHX33 protein levels in human normal lung tissues and malignant tissues. We found DHX33 highly expressed in multiple lung cancer samples as well as in numerous established lung cancer cell lines. Acute depletion of DHX33 protein caused defects in cell proliferation while also promoting apoptosis. Cancer cells with reduced DHX33 levels were unable to form tumors in xenograft

Received 31 May 2016 **Returned for modification** 28 June 2016
Accepted 30 August 2016

Accepted manuscript posted online 6 September 2016

Citation Yuan B, Wang X, Fan C, You J, Liu Y, Weber JD, Zhong H, Zhang Y. 2016. DHX33 transcriptionally controls genes involved in the cell cycle. Mol Cell Biol 36:2903–2917. doi:10.1128/MCB.00314-16.

Address correspondence to Hanbing Zhong, zhonghb@sustc.edu.cn, or Yandong Zhang, zhangyd@sustc.edu.cn.

B.Y. and X.W. contributed equally to this article.

Supplemental material for this article may be found at http://dx.doi.org/10.1128/MCB.00314-16.

models, implicating DHX33 as a potential new therapeutic drug target in treating NSCLC patients with a mutated Ras.

MATERIALS AND METHODS

Cell culture. H1299, Calu-1, Hcc827, and SK-LU-1 lung cancer cell lines were maintained in RPMI 1640 medium containing 10% fetal bovine serum (FBS), 2 mM L-glutamine, and streptomycin-penicillin. HeLa and BeaS2B cells were maintained in Dulbecco's modified Eagle's medium (DMEM) containing 10% FBS and streptomycin-penicillin. HEK293T cells were maintained in DMEM with 10% FBS and streptomycin-penicillin.

Lentivirus production. The targeting sequences of short hairpin RNAs (shRNAs) for human DHX33 are as follows (5′ to 3′): 1-shDHX33, CTCGGGAAACTTCCTCTGAAA; 2-shDHX33, GCTATCGCAAAGTG ATCATTT; 3-shDHX33, CATTTCCTTTAGAACCCAAAT. A pLKO.1 vector encoding an shRNA for a scrambled sequence (shSCR) was purchased from Addgene. To produce knockdown virus, 293T cells were transfected by pLKO.1-shRNA, pCMV-VSV-G (where CMV is cytomegalovirus and VSV-G is vesicular stomatitis virus G protein), and pHR8.2ΔR using Lipofectamine 2000 (Life Technologies) for virus packaging. To produce DHX33-overexpressing virus, 293T cells were transfected by pLVX-FLAG-DHX33, pCMV-VSV-G, and pHR8.2ΔR using Lipofectamine 2000 (Life Technologies) for virus packaging. Culture supernatants were harvested at 24 h and 48 h after transfection and then centrifuged at 2,000 rpm for 5 min.

Plasmids. The following primers were used to clone the promoter of human E2F1 gene into the NheI/XhoI site of the pGL3-control vector: forward primer, 5′-CAAATCGGCTAGCCGGGCTCAAGCAATCCTC-3′; reverse primer, 5′-AATTCCCTCGAGGGTCCCGGCCACTTTTACGC-3′. The following primers were used to clone the promoter of human cdc6 gene into the NheI/XhoI site of the pGL3-control vector: forward primer, 5′-CAA ATCGGCTAGCCGCACAGCCCCTGGCATAC-3′; reverse primer, 5′-AAT TCCCTCGAGGGCGAATGGCCACAGCGTTC-3′.

Immunoblotting. Whole-cell lysates were prepared by incubation with whole-cell lysis buffer that included 0.5% NP-40 and 1% SDS supplemented with Halt protease and phosphatase inhibitors (Sigma). Lysates were cleared by centrifugation, and the protein concentration was tested by a detergent-compatible (DC) assay (Bio-Rad). Lysates were boiled with SDS sample buffer, separated by SDS-PAGE, and transferred to polyvinylidene difluoride membrane (Millipore). Membranes were blocked in 5% nonfat dry milk and Tris-buffered saline plus Tween ([TBS-T] 10 mmol/liter Tris-HCl [pH 7.4], 150 mmol/liter NaCl, 0.1% Tween 20) buffer and incubated with primary antibodies diluted in blocking buffer at 4°C overnight. Blots were washed with TBS-T buffer and incubated with horseradish peroxidase (HRP)-conjugated secondary antibodies (1:10,000; GE Healthcare) in blocking buffer at room temperature. Immune complexes were visualized with an enhanced chemiluminescence kit (GE Healthcare). Primary antibodies for immunodetection were the following (source): antitubulin (goat; Santa Cruz), anti-DHX33 (Novus), anti-glyceraldehyde-3-phosphate dehydrogenase (anti-GAPDH; Bethyl), anticyclins (Santa Cruz), anti-E2F1 (Santa Cruz), and anti-MCM complexes (Abcam and Santa Cruz).

RNA sequencing. H1299 cells were infected by lentivirus encoding shSCR or 2-shDHX33. Three days after lentiviral infection, cells were harvested, and total RNA was extracted by Nucleospin RNA II kits. RNA samples were then further purified with magnetic oligo(dT) beads after denaturation. Purified mRNA samples were reverse transcribed into first-strand cDNA, and a second cDNA was further synthesized. Fragmented DNA samples were blunt ended and adenylated at the 3′ ends. Adaptors were ligated to construct a library. DNA was quantified by Qubit (Invitrogen). After cBot cluster generation, DNA samples were then sequenced by an Illumina HiSeq 2500 SBS instrument from Genergy Bio (Shanghai). Raw data were converted into Fastq format. The number of transcripts in each sample was calculated based on the number of fragments per kilobase of transcript per million fragments mapped (FPKM); Cuffnorm software was used to calculate the FPKM value for each sample, and the values were $\log_2$ transformed. Cuffdiff software was used to calculate the differential gene transcripts between different samples. For KEGG pathway analysis, the entire set of transcripts was used as the background list, the differential transcripts were used as the candidate list, and *P* was calculated. Significant genes were categorized based on gene functions.

Chromatin immunoprecipitation (ChIP). After cells were trypsinized and resuspended in complete medium, formaldehyde was added to a final concentration of 1% to cross-link DNA and its interacting proteins; this step was performed at room temperature for 10 min with a shaker. To stop cross-linking, 1.25 M L-glycine was added to a final concentration of 0.125 M; the mixture was shaken at room temperature for 5 min. After cells were washed with 1× phosphate-buffered saline (PBS), they were then resuspended in lysis buffer containing 1% SDS, 10 mM EDTA, and 50 mM Tris (pH 8.1) with protease and phosphatase inhibitors. To shear chromatin, cell lysates were sonicated extensively, centrifuged to pellet debris, and then diluted in buffer containing 0.5% NP-40, 50 mM Tris (pH 7.5), and 150 mM NaCl at a 1:5 ratio. Cell lysates were precleared by incubation with 2.5 μg of sheared salmon sperm DNA and 50 μl of protein A/G beads for 30 min at 4°C. Following incubation with 5 μg of antibody overnight at 4°C, 2.5 μg of sheared salmon sperm DNA and 50 μl of protein A/G beads were added, and samples were further incubated for 1 h. The beads were then washed twice in radioimmunoprecipitation assay (RIPA) buffer, twice in RIPA buffer containing 500 mM NaCl, and once with buffer containing 0.5% NP-40, 50 mM Tris (pH 7.5), and 150 mM NaCl. The beads were then extracted three times with a solution containing 1% SDS and 0.1 M $NaHCO_3$. To reverse the cross-linking, 6 M NaCl was added to the pooled extraction samples to a final concentration of 0.3 M, and samples were heated at 65°C for 5 h. DNA fragments were extracted by use of a Qiagen QuickSpin column and eluted. Quantitative PCR (qPCR) was performed with these purified DNA samples.

Apoptosis analysis. Apoptosis assays were performed with a Vybrant Apoptosis Kit 2 (Molecular Probes) according to the manufacturer's protocol.

Soft-agar assay. A total of 1.0×10^4 cells were mixed in 4.0 ml of 0.3% agar–DMEM–10% FBS as the top agar and plated on 60-mm plates with 4.0 ml of 0.6% agar–DMEM–10% FBS as the base agar. Plates were incubated at 37°C, checked every 3 days, and fed with 2.0 ml of 0.3% agar–DMEM–10% FBS every week. Colonies were photographed and counted 2 to 3 weeks later.

Immunohistochemistry (IHC). Human tumor tissue microarrays were purchased from US Biomax. This tissue microarray contained samples from 95 cases of lung cancer. A rabbit polyclonal anti-human DHX33 antibody was used at 1:50. Tissue slides were deparaffinized in xylene and rehydrated in a series of graded alcohols, and the antigen was retrieved in Tris buffer (pH 9.0) using a steamer. The sections were then treated with 1% hydrogen peroxide in methanol for 30 min to exhaust endogenous peroxidase activity. After a 1-h preincubation in 10% normal fetal bovine serum to prevent nonspecific staining, the samples were incubated with primary antibody at room temperature for 2 h. A standard protocol was then followed based on a Dako EnVision kit using polymer to amplify signals. Both immunoreactive intensity and the percentage of stained cells in different areas of the same slide were analyzed according to criteria described previously (15). DHX33 expression was scored as follows: 0, no staining; 1, weak; 2, moderate; and 3, strong. Additional points were scored as 1, 2, or 3 when the percentage of positive cells was less than 25%, 25% to 50%, or greater than 50%, respectively.

Bioluminescence imaging. Cells were plated in a six-well tissue dish and transfected with a pGL3-control promoter expressing firefly luciferase (F-luc). Twenty-four hours later, the cells were replated in 96-well plates, D-luciferin was added, and the plate was imaged with an IVIS-100 instrument. These cells were also harvested for total RNA extraction and analyzed by reverse transcription-PCR (RT-PCR) for determination of firefly luciferase (F-luc) transcript levels. To analyze firefly luciferase mRNA levels, the following primers were used: forward primer, 5′-CCC

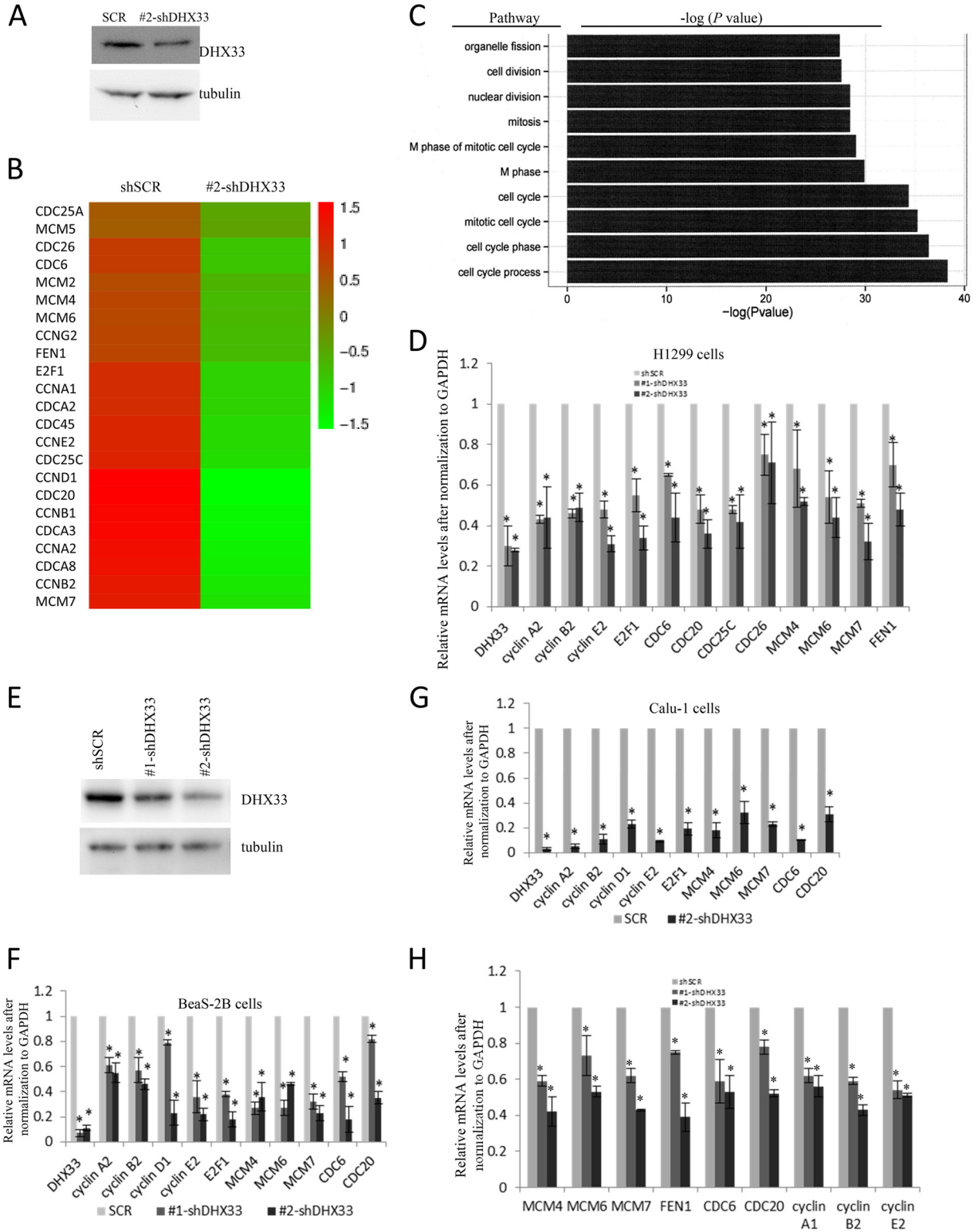

FIG 1 DHX33 transcriptionally controls genes involved in the cell cycle. (A) H1299 lung cancer cells were either infected with shSCR or 2-shDHX33 lentivirus. Four days post-lentiviral infection, cells were harvested. Whole-cell lysates were subjected to Western blot analysis with anti-DHX33 and antitubulin antibodies. (B) RNA sequencing was performed on the total RNA extracted. The heat map shows standardized expression levels for cell cycle genes. (C) Pathway analysis for significantly changed genes in DHX33 knockdown cells is shown. (D) H1299 lung cancer cells were infected with two different shRNAs targeting DHX33, with shSCR as a control. At 4 days post-lentiviral infection, cells were harvested. Total RNA was extracted and reverse transcribed into cDNA; qPCR was performed on these cells with the indicated primers. Bars indicate standard deviations from three independent analyses. All show statistically significant changes compared to levels in the scrambled control. *, $P < 0.05$ ($n = 3$). (E) Whole-cell lysates from H1299 cells after transduction by lentivirus encoding either shSCR or two shRNAs targeting DHX33. Whole-cell extracts were subjected to Western blot analysis with anti-DHX33 and antitubulin antibodies. (F) BeaS2B cells were

TGGTTCCTGGAACAATT-3′; reverse primer, 5′-GCAACCCCTTTTTG GAAACG-3′.

Recombinant DHX33 protein purification. The open reading frame of mouse DHX33 was cloned into the BamHI/HindIII sites in the pET32M-3C vector. The following primers were used to amplify DHX33 PCR products: forward primer, 5′-ATTATAGGATCCATGCCGGAGGA GGCGAGCCT-3′; reverse primer, 5′-ATAAATAAGCTTGTTTCTGGC CGTTCTCAGCTT-3′. Overexpressed wild-type recombinant DHX33 with a thioredoxin (Trx) tag at its N terminus and a 6×His tag at its C terminus was affinity purified from *Escherichia coli* through an Ni-nitrilotriacetic acid column (Qiagen).

Electric mobility shift assay (EMSA). Promoter sequences were PCR amplified and then enriched to obtain probes. To amply the mouse cyclin B2 promoter, the following primers were used: forward primer, 5′-TGT AAGGATGATGGACCAAGAGT-3′; reverse primer, 5′-TGGCAAGTGC GGACGAG-3′. To amply the mouse cdc20 promoter, the following primers were used: forward primer, 5′-GACCTGGATTCTTACCAACCTC-3′; reverse primer, 5′-AGCTCTCCCGAACACAAAC-3′. These probe DNA samples were biotin labeled according to the manufacturer's instructions (Invitrogen). Biotin-labeled promoter DNA samples were then incubated with or without DHX33 protein in the presence or absence of unlabeled probe according to a standard protocol. After incubation, DNA samples were separated by polyacrylamide gels and then transferred to nylon membrane. After UV cross-linking, streptavidin-HRP conjugates were added to the membrane to facilitate the detection of the labeled probes.

Zebrafish strains. The wild-type Tübingen line was maintained in a circulating aquaculture system according to the description in *The Zebrafish Book* (16). Embryos were incubated at 28.5°C and staged under standard conditions (17).

Cas9/gRNA design. The Cas9 and guide RNA (gRNA) plasmids were a generous gift from Bo Zhang of Perking University. These two plasmids were described previously (18, 19). For gRNA vector construction, gRNA oligonucleotides targeting the protein-encoding exon of the zebrafish *DHX33* gene (ENSDART00000156224) was selected using the ChopChop CRISPR/gRNA algorithm (http://chopchop.cbu.uib.no/). The sequence of target site is GGCCGCGCAGCGCAGACGCTTGG.

Whole-mount *in situ* hybridization. Digoxigenin-labeled antisense RNA probes were generated *in vitro* by using the zebrafish cDNA as a template with RNA polymerase (Promega, Madison, WI). Whole-mount RNA *in situ* hybridizations were performed essentially as described before (20).

Imaging. Pictures of zebrafish embryos were taken with an AxioImager A1 microscope and AxioCam digital camera (Zeiss, Oberkochen, Germany) and edited with Photoshop, version 7.0.

***In vitro* synthesis of capped Cas9 mRNA and gRNA.** The Cas9 plasmid was linearized by XbaI and used as the template for capped Cas9 mRNA synthesis with a mMESSAGE mMACHINE T7 kit (Ambion). This transcribed Cas9 mRNA was purified using an RNeasy minikit (Qiagen). For *DHX33* target guide RNA synthesis, we used the primers T7-cr fwd (5′-GAAATTAATACGACTCACTATA-3′) and Tracr rev (5′-AAAAAAA GCACCGACTCGGTGCCAC-3′) for the generation of the DNA templates of gRNA by PCR. The gRNA was transcribed *in vitro* with a T7 MAXIscript kit (Ambion), purified with a mirVana miRNA isolation kit (Ambion), and quantified by NanoDrop (Thermo). The size and quality of the resulting Cas9 mRNA and gRNA were confirmed by electrophoresis through a 2% agarose gel.

TABLE 1 Primers for qPCR analysis for human genes

Human gene product	Primer	Sequence (5′–3′)
hGAPDH	Forward	TGACAACGAATTTGGCTACA
	Reverse	GTGGTCCAGGGGTCTTACTC
DHX33	Forward	CGTCCTCCACAACCCTCCTT
	Reverse	AAAATTCTCTTTGCACCAATCCTT
Cyclin A1	Forward	ACACAGTTTCCCCTATGCTG
	Reverse	ATGCCTTCCGTGATGTCTG
Cyclin A2	Forward	TCCATGTCAGTGCTGAGAGGC
	Reverse	GAAGGTCCATGAGACAAGGC
Cyclin B2	Forward	AAAGTTGGCTCCAAAGGGTCCTT
	Reverse	GAAACTGGCTGAACCTGTAAAAAT
Cyclin D1	Forward	AAGCTGTGCATCTACACCGA
	Reverse	CTTGAGCTTGTTCACCAGGA
Cyclin E2	Forward	CTGCCTTGTGCCATTTTACC
	Reverse	GTCTTCAGCTTCACTGGACTAG
E2F1	Forward	ACCTCTTCGACTGTGACTTTG
	Reverse	GAGCATCTCTGGAAACCCTG
CDC6	Forward	TGGAAGCCTTTACCTTTCTGG
	Reverse	CCTCTTCCTGACAAATCTCCTG
CDC20	Forward	GATGTAGAGGAAGCCAAGATCC
	Reverse	AAGGAATGTAACGGCAGGTC
CDC25c	Forward	CCACTCAGCTTACCACTTCTG
	Reverse	ACCATTCGGAGTGCTACAAAG
CDC26	Forward	GGCCCTTAGTGTTGACTTCAG
	Reverse	CTCCTACAACTTCCACATCTTCC
MCM4	Forward	TTCTTTGACCGTTACCCTGAC
	Reverse	GGGATGTCCTGATCACCATG
MCM6	Forward	GTGATCAGGGATGTAGAACAGC
	Reverse	AGCTTGGGTCTCTTGAATACG
MCM7	Forward	GATGCCACCTATACTTCTGCC
	Reverse	TCCTTTGACATCTCCATTAGCC
FEN1	Forward	ACCCCGAACCAAGCTTTAG
	Reverse	CTCTTGATGTCATTCTCCCGG

Microinjection of zebrafish embryos and efficiency analysis. Cas9 mRNA (200 ng/μl) and gRNA (25 ng/μl) were coinjected into one-cell-stage wild-type embryos, and the total volume was 3 nl. After microinjection, embryos were raised in E3 medium at 28.5°C for examination of

transduced with either shSCR or shDHX33 lentivirus. Four days after lentiviral infection, cells were extracted for total RNA. qPCR analysis was performed to analyze the changes of the indicated cell cycle genes after normalization to GAPDH mRNA levels. Data were normalized to the level of the shSCR control. Data represent the average of three independent experiments; bars indicate the standard deviations from three separate experiments. *, $P < 0.05$ ($n = 3$). (G) A similar result was generated with Calu-1 lung cancer cells. Data were normalized to the level of the shSCR control. *, $P < 0.05$ ($n = 3$). (H) H1299 cells after virus infection were then pulsed by a uridine analog, 5-ethynyl uridine (EU), to label endogenous RNAs, followed by purification of labeled *de novo* RNAs by the use of a Click-iT nascent RNA capture kit. Purified RNA was converted into cDNA, and then qPCR was performed on these samples by the designated primers. Bars indicate standard deviations from three separate experiments. All showed statistically significant changes compared to control levels. *, $P < 0.05$ ($n = 3$).

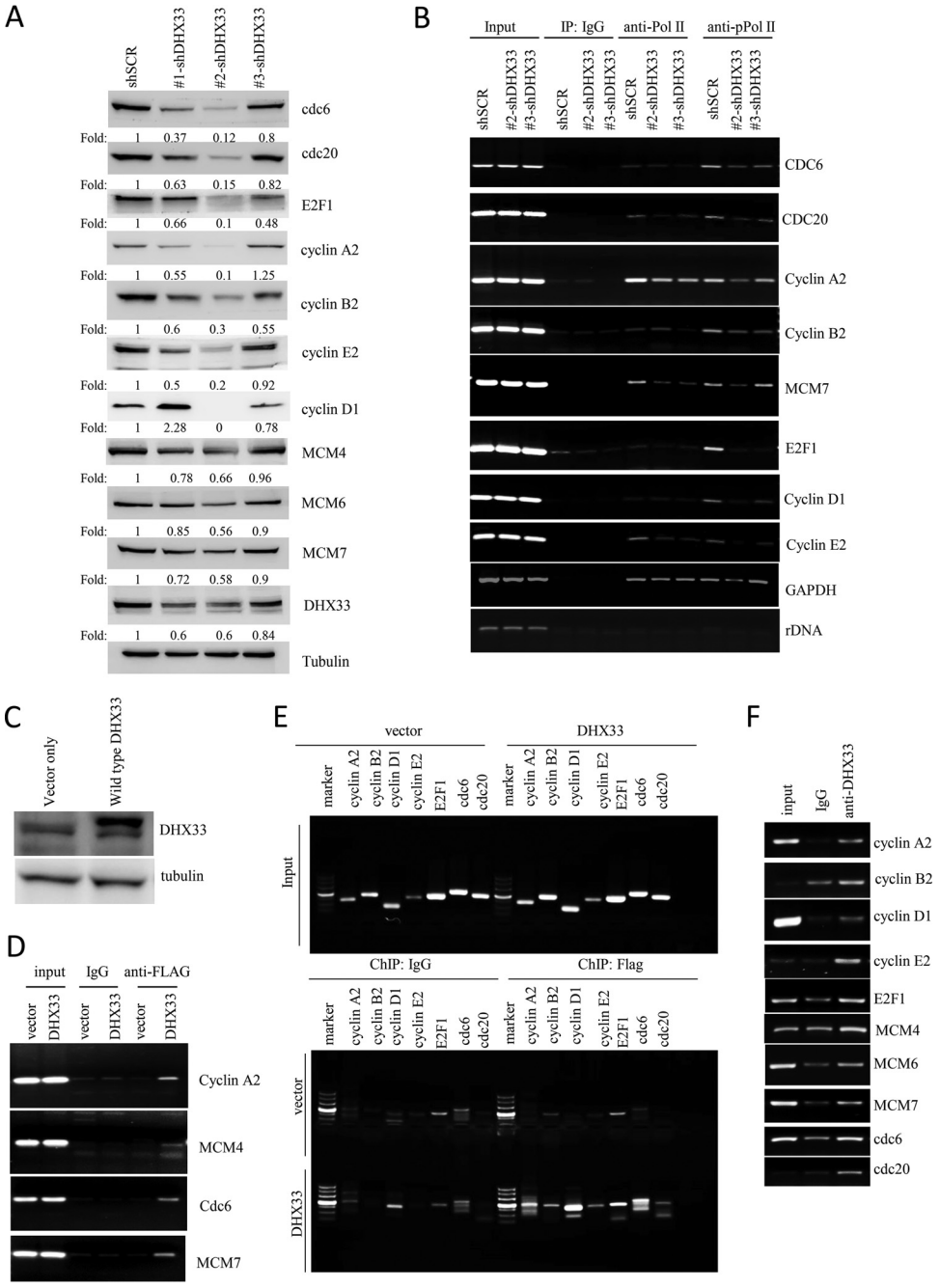

FIG 2 DHX33 promotes loading of active RNA polymerase II on cell cycle gene promoters and interacts with promoters of cell cycle genes. (A) H1299 lung cancer cells were infected with three different shRNAs targeting DHX33, with shSCR as a control. At 4 days post-lentiviral infection, cells were harvested. Whole-cell lysates were subjected to Western blot analysis with the indicated antibodies. Fold changes in expression levels were calculated after quantitation with ImageJ. (B) At 4 days after infection by lentivirus, the above-mentioned cells (shSCR, 2-sh-DHX33, and 3-shDHX33) were fixed by 1% formaldehyde, and then subjected to ChIP analysis with anti-Pol II, anti-pPol II (phosphorylation on S2 of the CTD), with IgG as a control. Samples were then analyzed by PCR and PAGE. A representative result is shown from three separate experiments. (C) H1299 cells were infected by lentivirus encoding either wild-type DHX33-FLAG or an empty vector. Western blotting was performed on the above-mentioned cells with the indicated antibodies. (D) At 4 days post-lentiviral infection, cells were cross-linked. Approximately equal amounts of sonicated cell lysates were used for total DNA extraction. The DNA samples were then analyzed by PCR, followed by PAGE for input analysis for all the indicated genes. ChIP analysis was performed on the above-mentioned cells; antibodies used in ChIP assays were anti-FLAG and IgG. Purified DNA fragments were analyzed by PAGE following PCR with the primer sets in Table 2 to detect the association of DHX33 with certain gene promoters. (E) Similar experiments were performed for analysis of DHX33 occupancy on the promoters of other genes. (F) H1299 cells were analyzed by ChIP analysis with anti-DHX33 (Santa Cruz) or IgG as a negative control. Purified DNA fragments were analyzed by PAGE following PCR with the primer sets in Table 2 to detect the association of DHX33 with the indicated gene promoters. IP, immunoprecipitation.

phenotypes. The efficiency of the mutations induced by Cas9/gRNA was evaluated by TA cloning and sequencing. Thirty embryos were collected for genomic DNA extraction for PCR at 24 h postfertilization (hpf); the PCR product was ligated with the pMD19-T vector (TaKaRa), and then about 10 positive clones were selected randomly to extract plasmids for sequencing. Primers used were the following: RV-M, AGCGGATAACA ATTTCACACAGGA; forward primer, TATACAAACCAAATCTGAAA CCC; reverse primer, TGCATACATCCTCTGTCAATAAA.

Quantitative PCR. The primers were purchased from Life Technologies. Total RNA was extracted by use of a NucleoSpin II (Clontech) RNA isolation kit and reverse transcribed into cDNA by use of a SuperScript III first-strand synthesis kit (Invitrogen). PCRs were performed with a Step One Plus thermal cycler. SYBR green mix from Bio-Rad was used for all quantitative real-time PCR (qRT-PCR) analyses. Transcript quantification was calculated based on the $\Delta\Delta C_T$ (where C_T is threshold cycle) method after normalization to GAPDH values. Melt curve analysis confirmed that single products were amplified. Three separate experiments were normally performed to obtain three sets of different RNA samples; qPCR data presented were the average of three different times, and the bars indicate the standard deviations (SD) calculated from these three data sets.

Mouse xenograft model. Nude female mice were purchased from Charles River Laboratories International, Inc., and received standard institutional care. They were at 5 weeks old at the time of surgery. For nude mouse injection, lung cancer cells were infected as indicated in Fig. 7J. Cells were trypsinized and resuspended in PBS at a concentration of 1×10^8 cells/ml. Five-week-old nude mice were injected subcutaneously with 1×10^7 cells along their flanks, with sample sizes of 5 mice per condition. At 6 weeks postinfection, tumors were dissected, photographed, and weighed. All mice were housed at the Southern University of Science and Technology Laboratory Animal Center. The experiments were performed by following standard protocols after approval by the university's Laboratory Animal Ethics Committee.

Statistical analysis. Data are presented as the means ± SD. Statistical significance was determined using a Student *t* test, with a *P* value of <0.05 considered significant.

TABLE 2 Primers for ChIP analysis of human gene promoters

Gene promoter	Primer	Sequence (5′–3′)
Cyclin A2 promoter	Forward	CCTGCTCAGTTTCCTTTGGTTT
	Reverse	AGCGGCGGCTGTTCTTG
Cyclin B2 promoter	Forward	TTGGGAATACAATGGAGAACTTACA
	Reverse	TCCGGGTTGCTCAGGGAT
Cyclin D1 promoter	Forward	GAAGGCAGCCCGAAGAGTC
	Reverse	TCCAGCAGCAGCCCAAGAT
Cyclin E2 promoter	Forward	GTGGTGGCGATCTTTCTT
	Reverse	TCCCTTGCTTCCTCTCTT
E2F1 promoter	Forward	CGCCACTTCATCGTATTGTAAAC
	Reverse	ATCTCCAACAGCCAACGTATAG
CDC6 promoter	Forward	GGGGAACCACATCTTGACACTT
	Reverse	TGAGGCCACGACCACTGAA
CDC20 promoter	Forward	TCTTCCAGATAGGCAGGTTTGA
	Reverse	CCAGAGCTACTTAGGGTACATTCCA
MCM4 promoter	Forward	CCAGAACGACTCGGGAAGC
	Reverse	CCCTGGCCGGTCATCAA
MCM6 promoter	Forward	GTCAGCACCACCACAATAA
	Reverse	CGGAGTAAGACTCTATGGAAGA
MCM7 promoter	Forward	GTAGACAAGAAGACGGCGAAAGT
	Reverse	GGGCGTCGGAAGGGAAT

RESULTS

DHX33 transcriptionally controls key genes involved in cell cycle progression and DNA replication. To investigate the mechanisms of how DHX33 promotes cell proliferation, we first analyzed the genome-wide gene transcription of H1299 cells. We performed RNA sequencing after DHX33 knockdown with scrambled knockdown sequences as a negative control (all changes in gene transcription are shown in Table S1 in the supplemental material). DHX33 knockdown efficiency is shown in Fig. 1A. We observed a significant change for numerous genes involved in cell cycle control following DHX33 knockdown (Fig. 1B). Pathway analysis indicated that the gene signature was most strongly associated with cell cycle control and cell division (Fig. 1C). We validated the mRNA expression changes of many genes by qRT-PCR, as shown in Fig. 1D. Two different shRNAs targeting the DHX33 gene were used, and the DHX33 knockdown efficiency is shown in Fig. 1E. We performed multiple RT-PCR analyses with two to three different shRNAs for DHX33 knockdown. All results consistently indicated that mRNA levels of the indicated genes (Fig. 1F and G) were significantly downregulated in H1299 cells. The primer sequences are shown in Table 1. To evaluate whether this change would occur in other cell lines, we analyzed the transcription levels for these genes in Calu-1 and BeaS2B cells after DHX33 knockdown. As shown in Fig. 1F and G, DHX33 knockdown also lowered the expression levels of key cell cycle genes expressed in these cells, too. Changes in the mRNA steady-state levels of the above-mentioned genes could be due to the decrease in newly synthesized mRNAs, or it could be due to accelerated mRNA decay. To study whether the reduction of the mRNA levels was due to a decrease in mRNA synthesis, we pulse-labeled endogenous RNAs for 30 min with the uridine analog, 5-ethynyl uridine (EU), followed by purification of labeled *de novo* RNAs. As shown in Fig. 1H, we found that, compared to level with the scrambled control, the levels of newly synthesized mRNAs for these genes were decreased significantly.

DHX33 is required for active RNA polymerase II recruitment to promoters of cell cycle genes. To investigate whether DHX33 loss would result in a concomitant decrease in protein levels for these cell cycle genes, we performed Western blot analysis with representative cell cycle proteins for H1299 cells that had been transduced either with shSCR or with shRNAs targeting DHX33. As shown in Fig. 2A, we found that DHX33 knockdown caused a marked reduction of the cell cycle proteins: cdc6, cdc20, cyclin A2, cyclin B2, cyclin E2, E2F1, MCM4, MCM6, and MCM7. This occurred roughly in a dose-dependent manner correlating with the degree of DHX33 knockdown efficiency, especially for cdc6, cdc20, cyclin B2, cyclin E2, MCM4, MCM6, and MCM7. We further studied the occupancy of RNA polymerase II and phosphorylated RNA polymerase II on the C-terminal domain (pS2-CTD) required for gene expression at designated gene promoters. With 2-shDHX33 and 3-shDHX33 targeting DHX33 in H1299 cells as shown in Fig. 2A, we found that DHX33 knockdown significantly reduced the abundance of phosphorylated RNA polymerase II at the cell cycle gene promoters (Fig. 2B). Compared to total RNA polymerase II, the occupancy of phosphorylated RNA

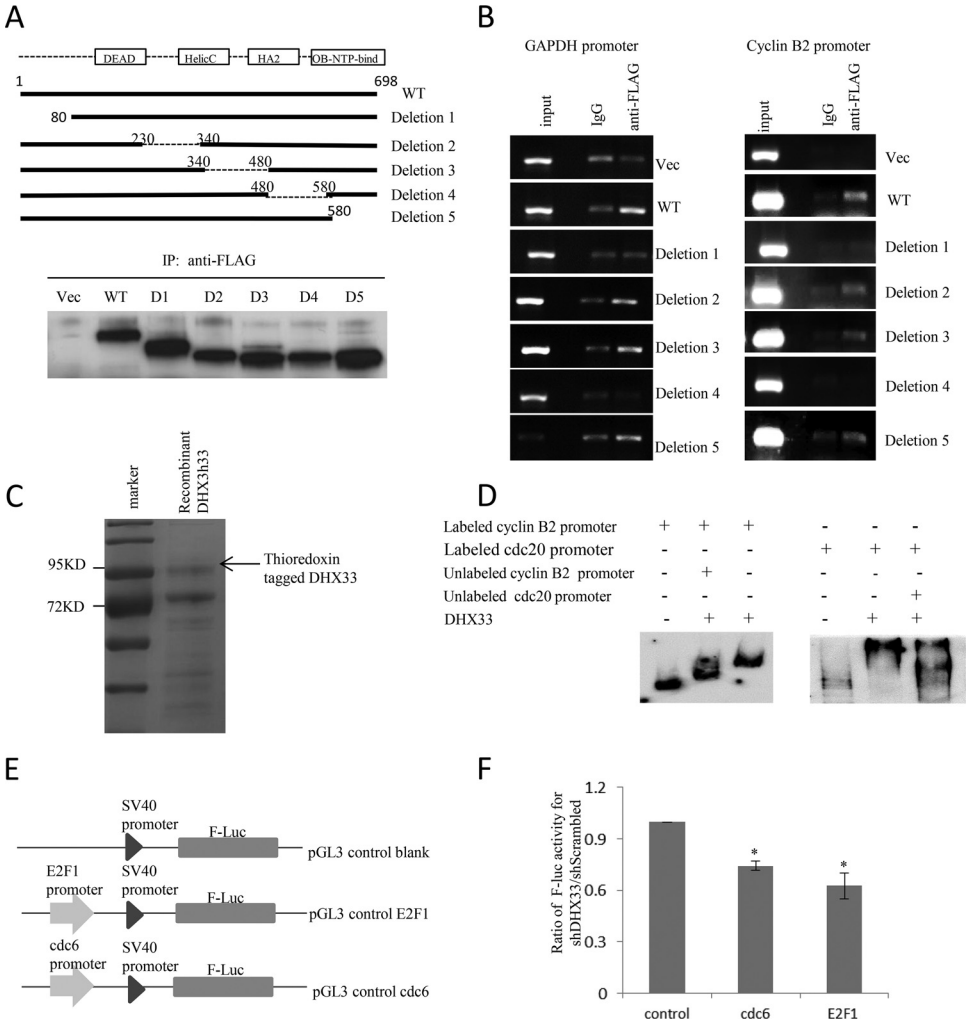

FIG 3 DHX33 directly binds on the promoters of cell cycle genes through amino acids 480 to 580 and positively regulates gene transcription. (A) Diagrams of the sequences of a panel of deletion mutants (D1 to D5 in the blot below) compared to the sequence of wild-type (WT) DHX33 are shown in the upper panel. Helic C, helicase C; OB-NTP-bind, oligonucleotide/oligosaccharide-nucleoside triphosphate binding. The Western blot shows the expression of each protein after immunoprecipitation (IP). Vec, vector. (B) H1299 cells were infected by lentivirus encoding either wild-type DHX33-FLAG or each of the deletion mutants, with an empty vector as a control. At 4 days post-lentiviral infections, cells were cross-linked. Approximately equal amounts of sonicated cell lysates were used for ChIP analysis. Purified DNA fragments were analyzed by PAGE following PCR with the primer sets to detect the association of DHX33 with GAPDH and cyclin B2 gene promoters. For GAPDH primers, we used GAPDH forward primer 5′-GCCACATCGCTCAGACACCAT-3′ and GAPDH backward primer 5′-CCCATACGACTGCAAAGACCC-3′. (C) SDS-PAGE analysis for isolated recombinant DHX33 protein from *E. coli*. (D) EMSA for promoters of cyclin B2 and cdc20 with DHX33 recombinant protein. (E) Diagrams of promoter-reporter constructs for E2F1 and the cdc6 gene. (F) H1299 lung cancer cells were infected with either shSCR or 2-shDHX33 lentivirus. At 2 days post-lentiviral infection, equal amounts of the promoter constructs were transfected into cells. Promoter activities for E2F1 and cdc6 were detected 24 h later by analyzing F-luc activity. Data presented is the relative ratio of the F-luc activities in shSCR to shDHX33 cells for each promoter-reporter plasmid. DNA transfection efficiency was normalized after quantitative PCR analysis. Experiments were repeated three times. SV40, simian virus 40. *, $P < 0.05$ ($n = 3$).

Pol II demonstrated more significant reduction in DHX33 knockdown cells. As a negative control, we analyzed the occupancy for RNA polymerase II on the ribosomal DNA (rDNA) promoter; we did not observe the interaction between rDNA and RNA polymerase II. However, when we analyzed the occupancy of RNA polymerase II on the GAPDH gene promoter, we found that the occupancy of phosphorylated RNA polymerase II was mildly decreased in 2-shDHX33 cells while the occupancy for the whole RNA polymerase II was kept almost the same. These results were consistent with the requirement of DHX33 for expression of these genes and indicated that DHX33 directly functions in transcriptional preinitiation complex assembly at their promoters.

DHX33 protein interacts with the promoters of genes involved in the cell cycle. To study whether the transcriptional control of cell cycle genes by DHX33 occurred directly or indirectly, we sought to determine whether DHX33 physically associated with these promoters. To observe DHX33 bound to these promoters, we performed chromatin immunoprecipitation experiments in H1299 cells. We first infected these cells with lentiviruses overexpressing either wild-type FLAG-DHX33 or an empty vector alone as a control. We checked the overexpression efficiency by Western blotting, (Fig. 2C). After cells were cross-linked with 1% formaldehyde and immunoprecipitated with anti-FLAG antibody (Fig. 2D and E), we discovered that DHX33 binds to the

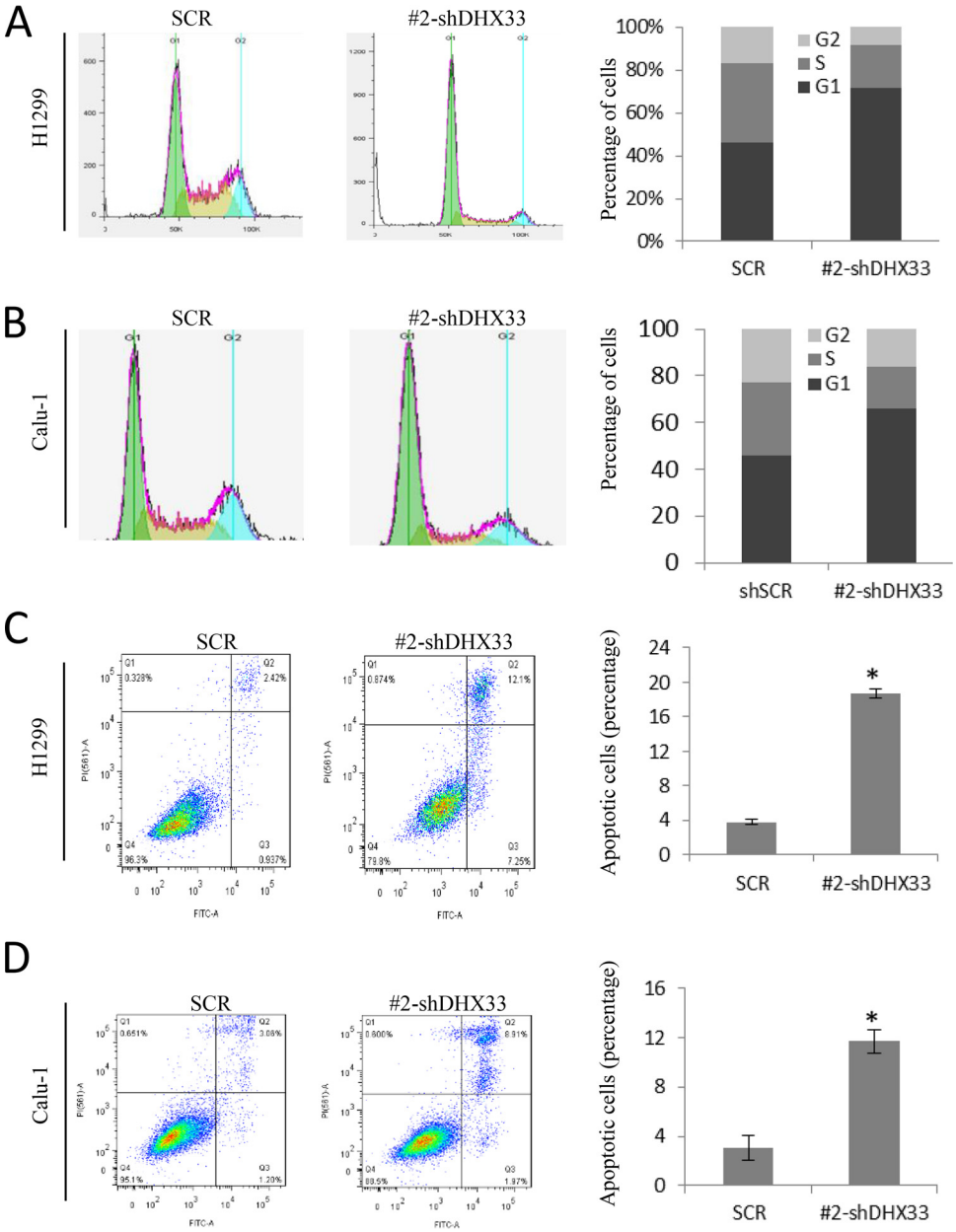

FIG 4 Acute DHX33 knockdown leads to cancer cell cycle arrest and apoptosis. (A and B) H1299 or Calu-1 cells were transduced with either shSCR or 2-shDHX33 lentivirus. At 4 days postinfection, cells were subjected to cell cycle analysis by flow cytometry after staining with propidium iodide. Quantitation of each cell cycle phase for both the scrambled control and DHX33 knockdown samples is shown. Experiments were repeated three times; a typical result is shown. (C and D) H1299 cells or Calu-1 cells were transduced with either shSCR or 2-shDHX33 lentivirus. At 5 days postinfection, cells were subjected to apoptosis analysis by flow cytometry with a Vybrant apoptosis kit after PI labeling of nuclei and fluorescein isothiocyanate labeling of annexin V. The percentage of cells is shown in each quadrant. The number of apoptotic cells was calculated and graphed. Bars indicate standard deviations from three separate analyses.*, $P < 0.01$ ($n = 3$).

promoter region of many genes involved in the cell cycle and in cell division, including the MCM4, MCM7, cdc6, cdc20, cyclin A2, cyclin B2, cyclin D1, cyclin E2, and E2F1 genes. These results provide evidence that DHX33 physically interacts with these gene promoters and thereby directly promotes the loading of active RNA polymerase II to initiate gene transcription. Furthermore, we also performed chromatin immunoprecipitation analysis for endogenous DHX33, and as shown in Fig. 2F, endogenous DHX33 interacts with the promoters of this group of genes. The primers for ChIP analysis are shown in Table 2.

DHX33 interacts with gene promoters through the domain of residues 480 to 580. To further investigate which domain of DHX33 is critical in binding to gene promoters, we performed chromatin immunoprecipitation analysis with deletion mutants of DHX33 as shown in Fig. 3A and B. We found that the domain of residues 480 to 580 is important in mediating the protein-DNA interaction. To study whether the interaction between DHX33 and DNA is direct, we performed an EMSA (Fig. 3C and D). We first isolated thioredoxin-tagged DHX33 from *E. coli*, and then protein purity was checked by SDS-PAGE (Fig. 3C). After cells

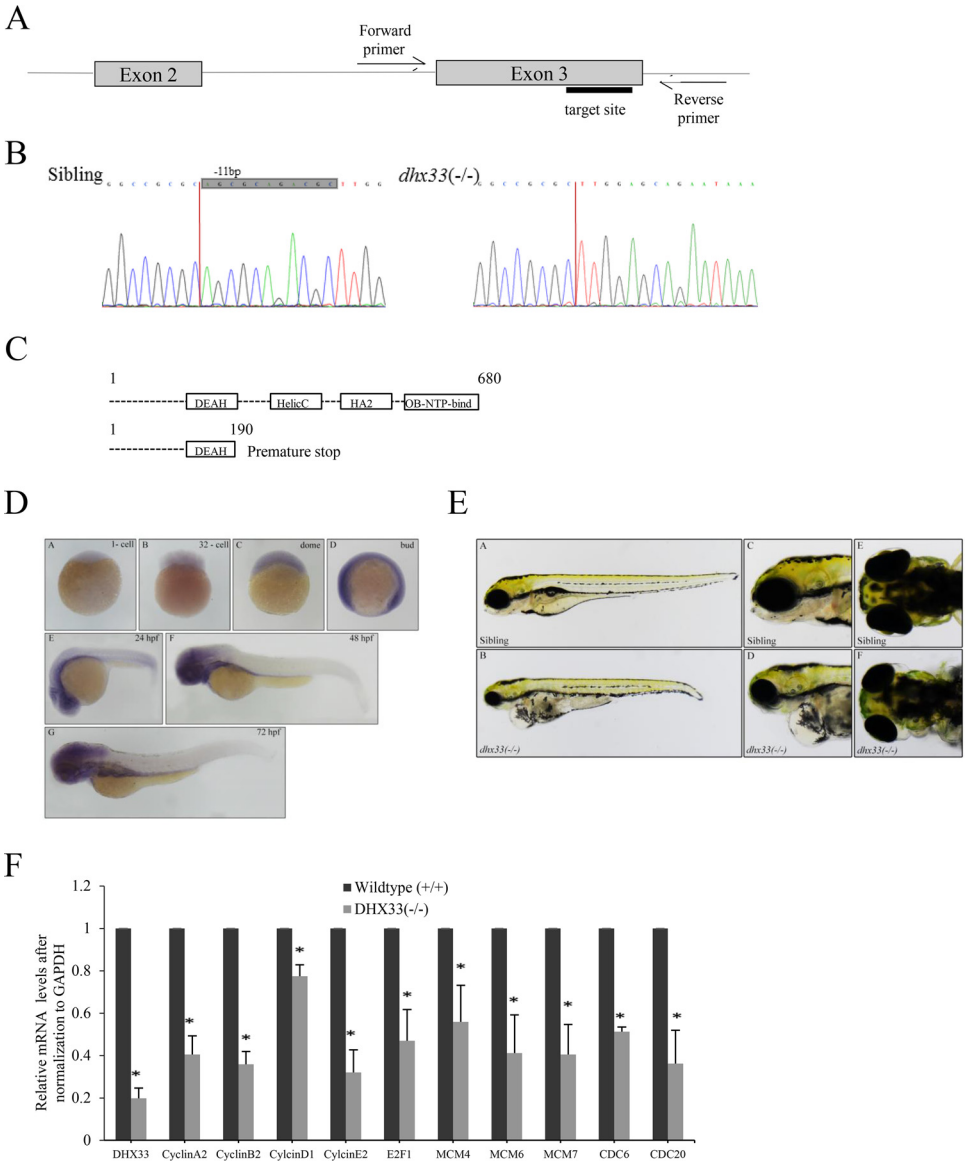

FIG 5 DHX33 gene knockout causes severe developmental defects due to downregulation of cell cycle genes in zebrafish. (A) CRISPR/Cas9 gene targeting site (black bar) on exon 3 of DHX33. Both forward and reverse primers are shown in the gene sequence for screening the mutant clones by PCR. (B) The sequencing results for both the sibling and the DHX33 mutants on exon 3. Highlighted are the 11 bp missing in the DHX33 mutants. (C) The 11-bp deletion causes a reading frame shift, and the putative mutated DHX33 protein has a premature stop codon and becomes a truncated protein with 190 amino acids. (D) The expression pattern of DHX33 in zebrafish. A whole-mount *in situ* hybridization was performed for zebrafish embryo development. The stages are labeled on the top right corner of each frame. Before 24 hpf, DHX33 is expressed universally; after 24 hpf, expression is gradually restricted in neural tissue and digestive tissue. (E) A DHX33 homozygous mutant at 96 hpf. Mutant embryos develop more slowly than those of siblings. Their heads and eyes are much smaller. Frames A to D show side views; frames E and F are dorsal views. (F) The mRNA levels of the indicated genes were analyzed by qPCR. Embryos were collected at 4 days postfertilization, and total RNA was extracted. Bars indicate standard deviations from three separate experiments. *, $P < 0.05$ ($n = 3$).

were incubated with biotin-labeled cyclin B2 or cdc20 gene promoters, we found a significant band shift, which was somehow reversed by coincubation with a 2-fold amount of unlabeled probes. To study whether the absence of DHX33 would decrease the promoter activity of the above-mentioned genes, we cloned E2F1 and cdc6 proximal promoters (~1 kb upstream of start codon) into the pGL3-control plasmid. A schematic of these plasmids is shown in Fig. 3E. After the constructs were transfected into either control cells or DHX33 knockdown cells, we found that the promoter activities for both E2F1 and cdc6 were decreased (Fig. 3F).

DHX33 protein deficiency triggers cancer cell cycle arrest, reduction in DNA replication, and apoptosis. We previously found in wild-type mouse embryonic fibroblasts and primary human fibroblasts that DHX33 loss would cause cell cycle arrest at the G_1/S boundary in a p53-dependent manner (3). Here, in H1299 cells that express mutant p53 and in Calu-1 cells that have a p53 deletion, we analyzed whether DHX33 deficiency would cause cell cycle arrest independent of p53 function. As shown in Fig. 4A and B, loss of DHX33 caused a significant increase of G_1-phase cells and a marked reduction in S-phase cells, indicating that cell cycle arrest in the G_1/S-phase transition in lung cancer

cells occurs independent of p53. To analyze whether DHX33 loss would decrease DNA replication due to a reduction of MCM proteins, we analyzed the stability of an episomal plasmid in cancer cells. The plasmid encodes both the EBNA1 gene and OriP, which functions as a DNA replication of origin. OriP plasmids can link to chromosomes during mitosis and segregate to daughter cells without integration into host chromosomes. As this plasmid contains a hygromycin selection marker, cells can be selected by hygromycin. We transfected this plasmid into both the scrambled and DHX33 knockdown cells and then selected them in either puromycin or hygromycin-puromycin medium. In contrast to results with the shSCR control, we found that DHX33 knockdown caused decreased cell survival in this setting, indicating that DHX33 is important in DNA replication (data not shown).

To evaluate whether loss of DHX33 would lead to cell death, we performed apoptosis assays by annexin V/propidium iodide (PI) costaining. Annexin V-positive cells are early apoptotic cells while annexin V/PI-double-positive cells are late apoptotic cells. By calculating the cells in the upper right and lower right quadrants in the graphs shown in Fig. 4C and D, we can evaluate the effect of DHX33 loss on apoptosis in both H1299 and Calu-1 cells. Importantly, we found that in both cell types, acute depletion of DHX33 caused significant cell death through apoptosis, as shown in Fig. 4C and D. Six days after lentiviral infection, DHX33 knockdown caused the apoptotic index to increase from 3% to approximately 12 to 20% compared to control levels.

DHX33 gene knockout causes severe developmental defects and downregulation of cell cycle genes in zebrafish. To further investigate whether DHX33 promotes gene transcription *in vivo*, we chose zebrafish as a model system. The DHX33 homolog in zebrafish has up to 71% sequence identity and 83% sequence similarity with the human DHX33 protein. We designed a guide RNA to specifically target the third exon of the DHX33 homolog gene and utilized CRISPR/Cas9 to edit the genome DNA sequence for the DHX33 gene. We obtained a clone with a deletion of 11 bp in exon 3. This deletion caused a frameshift in the open reading frame, introduced a premature stop codon, and resulted in the production of a truncated DHX33 without an RNA helicase core domain (Fig. 5A to C). We also performed whole-mount RNA-fluorescence *in situ* hybridization (FISH) analysis for DHX33 gene expression during the course of zebrafish embryo development. We found DHX33 to be a ubiquitous protein in embryos before 24 hpf (hours postfertilization) and gradually restricted to neural tissue and the digestive tract (Fig. 5D). Heterozygotes for this DHX33 mutant have no obvious phenotypes; they are fertile and appear to be normal. For DHX33 homozygote mutants, until 48 hpf, the appearance of the mutant embryo was nearly normal. After 48 hpf, the mutant embryo developed more slowly than siblings. At 96 hpf, mutant embryos were smaller, especially head and eyes, and had heart edema (Fig. 5E). Mutant embryos died eventually. We purified the total RNA from these mutant embryos on day 3 postfertilization and analyzed the mRNA levels for genes involved in the cell cycle. As shown in Fig. 5F, we found that all previously analyzed cell cycle genes were significantly downregulated in the mutants compared to the levels in the wild-type zebrafish. The primer sequences are shown in Table 3. This result confirmed previous findings by providing the evidence *in vivo*.

DHX33 protein expression in non-small-cell lung cancers. To study the possible role of DHX33 in cancers, Western blot analysis was used to measure DHX33 protein expression in four non-small-cell lung cancer cell lines; these results were then compared to those in BeaS2B and HeLa cells, where we found DHX33 protein to be highly expressed. As shown in Fig. 6A, after normalization by γ-tubulin protein levels, DHX33 was found to be highly expressed in three out of four non-small-cell lung cancer cell lines. Two of these lines, H1299 and Calu-1, are K-Ras-mutated cancer cell lines. We found that DHX33 protein levels correlated with the doubling times (Fig. 6B). We observed only mild changes in the mRNA levels of DHX33 in non-small-cell lung cancer tissues compared to levels in normal samples using public Oncomine data sets (Fig. 6C). We further performed immunohistochemistry staining for DHX33 with a set of human non-small-cell lung cancer tissue arrays. Our results indicated that DHX33 was highly expressed in 30% of the 95 lung cancer cases while normal lung tissues all exhibited weak staining for DHX33. Images of all of the DHX33-positive tumor tissues, the representative normal tissues, and the negative tissues are shown in Fig. 6D and E. The detailed tumor type, stages, and scores are summarized in Table 4. Statistical analysis from IHC is shown in Table 5 and clearly shows that DHX33 expression correlates with tumor stages and ages, implying that DHX33 may function to promote tumor formation. Additionally, we performed another lung cancer tissue array with

TABLE 3 Primers for qPCR analysis of zebrafish genes

Zebrafish gene product	Primer[a]	Sequence(5′–3′)
GAPDH	FP	GCTTCTCACAAACGAGGACACA
	RP	GTCAAGAAAGCAGCACGGGT
DHX33	FP	TGCCGCTCTACGCCTCACT
	RP	GCAATGTTGGTGGACAGAATCA
Cyclin A2	FP	GCGGGAAATGGAGGTCAAG
	RP	TCCCACTTCCACCAACCAGT
Cyclin B2	FP	CACAAACCAGTTCAGACAAAGAAGG
	RP	GCTGGACCTGGGCACTTTTG
Cyclin D1	FP	GAACACTTCCTTGCCAAACTGC
	RP	GTCGGTGCTTTTCAGGTACAGTC
Cyclin E2	FP	CCCGCAACACATTACAAGAAAG
	RP	TAAGACACTGGCACTAACATCACC
E2F1	FP	GCAACGCCACATCATACAAGC
	RP	CGTAGCGGGATTTCTCCACA
MCM4	FP	GAACGCTGGTCTGGATCTCAA
	RP	CGCTGTAGGGTCGCACTTG
MCM6	FP	ACGAAGGTTTGCGTGGGC
	RP	CTGGTGCAGAGGTTATGGTAGAGG
MCM7	FP	GGTTGTGCGTGATGTGAAGGC
	RP	ATGATGAGCGGCGTGAAGC
CDC6	FP	GTGTTCCTCAAGTGGCTCGG
	RP	CTTCACACAGCTTGCCCAACT
CDC20	FP	GCCCTCTACTGCGCCAAATC
	RP	ATAACCCTCTGGTGCGTAAAGC

[a] FP, forward primer; RP, reverse primer.

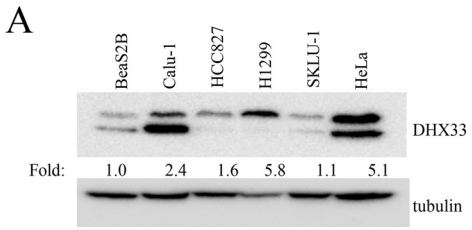

B

cell line	doubling time
BeaS2B	26 hours
Calu-1	24 hours
H1299	19 hours
HCC827	30 hours
SKLU-1	26 hours
HeLa	18 hours

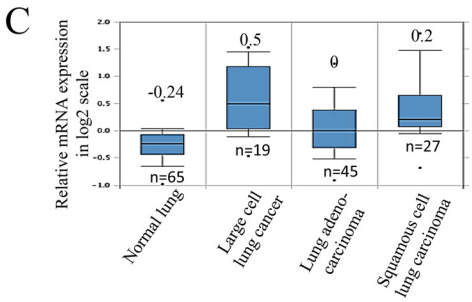

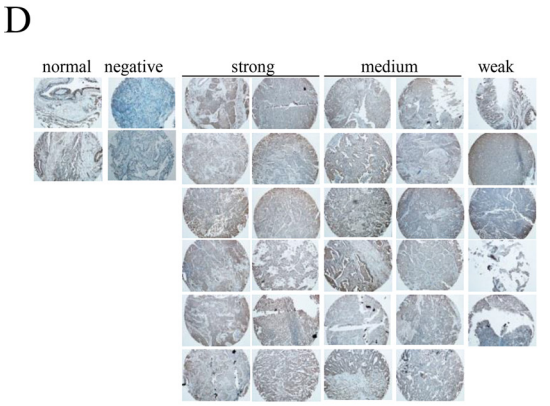

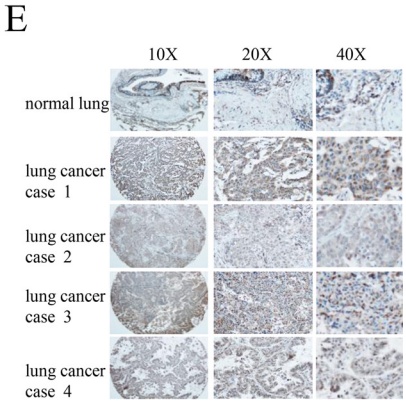

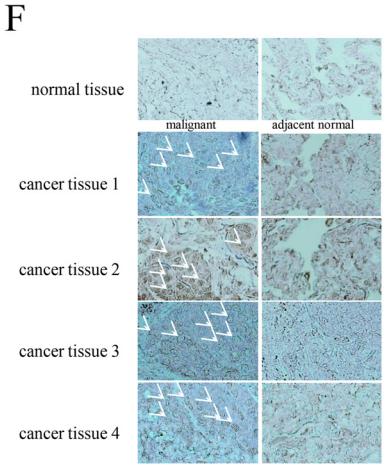

FIG 6 Overexpression of DHX33 in Ras-mutated lung cancer cell lines and non-small-cell lung cancers. (A) A panel consisting of four different lung cancer cell lines, the normal lung epithelial cell line BeaS2B, and HeLa cells was analyzed for DHX33 protein expression by Western blotting. A total of 50 μg of whole-cell extracts was used for analysis. Tubulin was used as a loading control. Quantitation of the signal was made by ImageJ software and normalized by tubulin levels. (B) Equal numbers of the indicated lung cancer cell lines were plated, and cells were counted on a daily basis. Doubling times were estimated based on the growth curves. (C) Analysis of DHX33 mRNA expression in non-small-cell lung cancers using the Oncomine database (36). Oncomine was searched for non-small-cell lung cancer data sets in which DHX33 mRNA levels exhibited significant differences (*t* test, *P* value of <0.001) in cancer versus normal tissue. The graphs show box plots of a data set comparing the cancer and normal samples. The 25th to 75th percentiles are indicated by a filled box, with the median indicated by a horizontal line, and the value of the median is indicated on top; the number of each type of tissue sample is shown at the bottom. (D) Immunohistochemistry was performed on a human tissue array, including samples from 95 cases of various stages of non-small-cell lung cancers tissues and three normal lung tissue samples. Brown indicates positive DHX33 expression; blue demarcates nuclei by eosin staining. All positive tissues are presented and are categorized into DHX33 strong, DHX33 medium, and DHX33 weak groups. All images were taken at a magnification of ×10. Data are summarized in Tables 4 and 5. (E) Representative images at various magnifications to show positive and strong nucleus staining of DHX33. (F) Immunohistochemistry was performed on a human tissue array, including 45 pairs of malignant non-small-cell lung cancer tissue specimens, an adjacent normal specimen, and 10 normal tissue samples. Typical images of normal, adjacent normal, and malignant lung cancer tissues are shown. All images were taken at a magnification of ×20. Arrows indicate punctate nucleolus staining.

TABLE 4 List of DHX33-positive lung cancer tissues with patient pathological data and IHC score

Sample no.	Patient age (yr)	Tumor type	Stage[a]	Score[b]
1	62	Squamous cell carcinoma	T2N1M0	3 + 2
2	60	Squamous cell carcinoma	T3N3M0	3 + 3
3	47	Bronchioloalveolar carcinoma	T2N0M0	3 + 3
4	77	Squamous cell carcinoma	T2N1M0	3 + 2
5	56	Squamous cell carcinoma	T2N1M0	3 + 2
6	56	Squamous cell carcinoma	T2N0M0	2 + 3
7	76	Squamous cell carcinoma	T2N1M0	2 + 3
8	53	Undifferentiated carcinoma	T2N0M0	2 + 2
9	51	Undifferentiated carcinoma	T2N2M0	3 + 3
10	55	Bronchioloalveolar carcinoma	T2N0M0	3 + 2
11	58	Adenosquamous carcinoma	T2N0M0	3 + 2
12	70	Adenocarcinoma	T3N1M0	3 + 2
13	73	Squamous cell carcinoma	T2N0M0	2 + 2
14	74	Bronchioloalveolar carcinoma	T3N0M0	2 + 2
15	66	Adenocarcinoma	T2N0M0	2 + 2
16	74	Bronchioloalveolar carcinoma	T4N0M0	2 + 2
17	50	Squamous cell carcinoma	T2N0M0	2 + 2
18	42	Bronchioloalveolar carcinoma	T2N1M0	2 + 2
19	75	Adenosquamous carcinoma	T2N0M0	2 + 2
20	40	Squamous cell carcinoma	T2N1M0	1 + 3
21	55	Undifferentiated carcinoma	T2N0M0	1 + 3
22	59	Adenosquamous carcinoma	T4N1M0	2 + 2
23	63	Adenosquamous carcinoma	T2N1M0	2 + 2
24	64	Bronchioloalveolar carcinoma	T3N0M0	1 + 3
25	65	Adenocarcinoma	T2N1M0	2 + 1
26	63	Small cell carcinoma	T2N0M0	1 + 3
27	70	Bronchioloalveolar carcinoma	T3N1M0	1 + 2
28	51	Adenosquamous carcinoma	T3N1M0	2 + 1

[a] Stages are indicated according to the generally accepted TNM (T, tumor; N, node; M, metastasis) system.
[b] The first number indicates the DHX33 expression level as follows: 0, no staining; 1, weak staining; 2, moderate staining; 3, strong staining. The second score represents the percentage of positive cells, scored as 1, 2, or 3 when the percentage of positive cells was less than 25%, 25% to 50%, or greater than 50%, respectively.

more normal tissue controls. This tissue array contained 45 samples of paired non-small-cell lung cancer tissue, adjacent normal lung tissue, and 10 normal lung tissues. We found DHX33-positive nucleolus tissues in a substantial number of non-small-cell lung cancer samples; DHX33 was expressed in the nucleoli of 9 out of 45 lung cancer tissues but not in the nucleoli of adjacent normal lung tissues (Fig. 6F).

TABLE 5 Statistical summary of IHC staining results according to tumor subtypes and stages

Parameter	No. of positive tissues (%)
Tumor subtype	
Squamous cell carcinoma	9/49 (18.4)
Adenocarcinoma	3/18 (16.7)
Bronchioloalveolar	7/11 (63.6)
Adenosquamous carcinoma	5/9 (55.6)
Undifferentiated carcinoma	3/5 (60)
Small-cell carcinoma	1/3 (33.3)
Tumor stage	
I-II	20/74 (27)
III	6/17 (35)
IV	2/5 (40)
Patient age (yr)	
<50	3/19 (15.8)
50–60	11/50 (22)
60–70	8/20 (40)
>70	6/13 (46.2)

DHX33 promotes NSCLC cell proliferation and tumor development *in vitro* and *in vivo*. To evaluate the consequences of DHX33 depletion in lung cancer cells, we used small interfering RNAs through lentivirus delivery to stably knock down DHX33 in DHX33 highly expressing lung cancer H1299 and Calu-1 cells. We then analyzed several cellular processes, including cell proliferation and anchorage-independent cell growth. As shown in Fig. 7A and B, after DHX33 depletion, these cancer cells had lost many of their proproliferative phenotypes. This was observed in both long-term focus formation and the short-term growth curve analysis (Fig. 7A to C). When the cells transduced with the scrambled control and the two shRNAs targeting DHX33 were compared, we found that 2-shDHX33 had better knockdown efficiency than 1-shDHX33, and, similarly, more impact on cell proliferation, indicating a dose-dependent effect. The ability to grow in an anchorage-independent manner is a hallmark of cancer cells. We performed this analysis in both H1299 and Calu-1 cells. DHX33 knockdown caused a significant reduction in soft-agar colonies, as demonstrated in Fig. 7D and E. To further evaluate whether DHX33 promotes lung cancer growth *in vivo*, we used mouse xenograft models to study the effect of DHX33 knockdown on tumor growth. Two days after lentiviral infection of lung can-

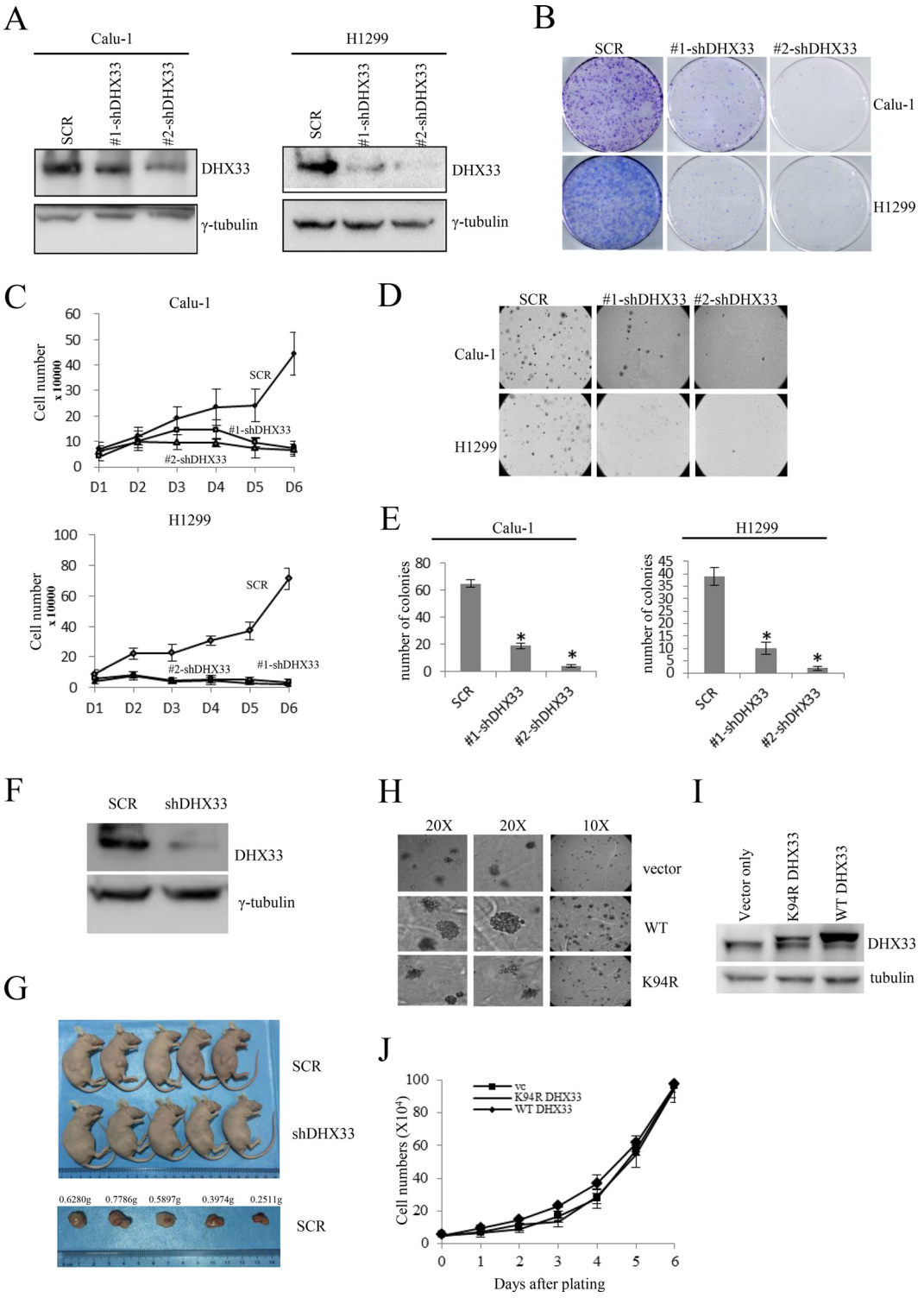

FIG 7 DHX33 promotes NSCLC proliferation and tumor development *in vitro* and *in vivo*. (A) Calu-1 and H1299 lung cancer cells were infected with either shSCR or shDHX33 lentivirus. At 4 days post-lentiviral infection, cells were harvested. Whole-cell lysates were subjected to Western blot analysis with anti-DHX33 and antitubulin antibodies. (B) At 3 days postinfection, cells were split, and approximately 5,000 cells per condition were plated on a 100-mm dish in triplicates. Cells were further cultured for 2 weeks until they were subjected to focus analysis. Typical images for the culture of the indicated transduced cells are shown. (C) The above-mentioned cells were trypsinized; equal numbers of cells were plated onto six-well plates, and cells were counted on a daily basis. Bars indicate standard deviations from three separate counts. (D) Calu-1 and H1299 cells were transduced with either shSCR or shDHX33 lentivirus. Cells were then subjected to soft-agar analysis after and plated at 1×10^4 into each 60-mm dish. A typical image is shown after culturing for 2 weeks. (E) Quantitation of colony numbers in the soft-agar assay. Error bars were based on results from triplicates. *, $P < 0.05$ ($n = 3$). (F) Western blotting was performed for H1299 cells after lentiviral infection to detect DHX33 knockdown efficiency. (G) A group of 5 nude mice were injected in their flanks on one side with H1299 cells transduced with either shSCR or shDHX33 (10^7 cells per injection). Tumors were dissected after 6 weeks, and images were taken before and after tumor removal. Tumor weight is labeled in the tumor images. (H) H1299 cells were infected by lentivirus encoding vector only, wild-type DHX33, and K94R mutant DHX33. Cells were then plated for soft-agar analysis. Typical images after 14 days of culture incubation are shown. (I) A Western blot is shown for H1299 cells for overexpression of the indicated proteins. (J) Growth curves were generated over a 6-day period; bars indicate standard deviations from three separate counts for each sample. vc, vector.

cer cell lines, equal numbers of these cells were subcutaneously injected into immunocompromised mice. Six weeks after injection, the control group of immunocompromised mice, in which we showed that the DHX33 levels were normal, demonstrated rapid tumor growth while the DHX33 knockdown group exhibited no detectable tumor, as shown in Fig. 7F and G. To check the effects of DHX33 overexpression on cancer cell growth, we overexpressed either a K94R helicase-defective mutant or the wild-type DHX33 in H1299 cells. As shown in Fig. 7H to J, we found that overexpression of the wild-type DHX33 caused an enhancement of anchorage-independent growth and a mild increase in cell proliferation of H1299 cells. Our results clearly show that DHX33 is required for lung cancer cell line growth *in vitro* and tumor formation *in vivo*.

DISCUSSION

We report here for the first time that DHX33 binds to the promoter regions of cell cycle genes such as the cyclin A2, cyclin B2, cyclin E2, MCM4, MCM7, cdc6, cdc20, and E2F1 genes. DHX33 deficiency caused dramatic decreases in the transcription levels of these genes. We found that DHX33 deficiency caused cell cycle arrest at G_1/S and apoptosis independent of p53. Additionally, DHX33 physically interacted with these cell cycle gene promoters, recruiting active RNA polymerase II loading onto the promoters of the above-mentioned cell cycle genes. Moreover, by using the zebrafish model, we found that DHX33 actively regulates genes involved in the cell cycle *in vivo*, and this is very important for embryo development. DHX33 null mutants showed severe developmental defects in the brain and in the eye; all homozygous DHX33 mutant embryos died by 7 days postfertilization.

DHX33 was found to be overexpressed in Ras-mutated human lung cancer cell lines and a subset of human lung cancers. This is consistent with previous findings that DHX33 is a downstream target of Ras. DHX33 was found to be pivotal for proliferation and growth both *in vitro* and *in vivo*. DHX33 was found to be a critical transcriptional regulator of cell cycle control genes. Acute knockdown of DHX33 caused apoptosis in lung cancer cells but not in immortalized normal lung epithelial cells. We previously observed that in wild-type mouse embryonic fibroblasts (MEFs) and human primary fibroblasts, the majority of cells were arrested in G_1/S-phase transition after DHX33 depletion (3, 7) and that this was dependent on p53 function. Our study with lung cancer cells indicates that DHX33 deficiency causes cell cycle arrest or apoptosis independent of p53. We have previously found DHX33 to be a protein capable of associating with chromatin (3). In this study, we performed ChIP assays/EMSAs and found that DHX33 readily interacted with promoters of numerous important cell cycle-regulatory genes, whose transcriptional upregulation has been reported in human cancers. It would be worthwhile to perform a global ChIP sequencing analysis for DHX33 protein in different cell types and tissues to determine the global extent to which DHX33 directly influences transcription. Further in-depth ChIP sequencing should be able to identify the specific regions of gene promoters that DHX33 binds to. This is not the first time that DEAD/DEAH box proteins have been found to regulate gene transcription. Recently, a study showed that DDX21 binds 7SK RNA and is recruited to the promoters of Pol II-transcribed genes encoding ribosomal proteins and snoRNAs (21). Our results further strengthen the concept that DEAD/DEAH box proteins cannot only influence RNA metabolism but also shape DNA transcription.

Our report on DHX33 underscores its importance as a druggable target in treating Ras-mutated lung cancer patients. Mutation of Ras occurs frequently in not only lung cancers but also a variety of other types of cancers. Successfully targeting Ras has proven difficult in the clinic (22, 23). Given the difficulty in designing potent clinical inhibitors for Ras, key downstream effectors of Ras might provide alternative, promising therapeutic targets for the treatment of Ras-mutated cancers (24). Our study here demonstrates that DHX33 is an important factor downstream of Ras for tumor formation. By inhibiting DHX33 through the introduction of small interfering RNAs, Ras-mutated human cancer cells lost their tumorigenicity and rapidly succumbed to apoptosis. Therefore, our findings offer DHX33 as a possible target for the future treatment of Ras-mutated human cancers. However, given the essential role of DHX33 in normal cell proliferation, excessive use of inhibitors for this protein may have a potential for toxicity to normal tissues.

The family of DEAD/DEAH box RNA helicases belongs to a large family of multifunctional proteins involved in various steps of RNA metabolism (25). Many characterized RNA helicases have been found to be fundamental in essential cellular processes (1, 26). In recent years, a few RNA helicases have been found to participate in cancer development even though their detailed molecular mechanisms remain largely undiscovered (27–33). Furthermore, despite the characterization of several DEAD/DEAH proteins, few specific inhibitors targeting these ATP-dependent helicases have been developed. Several lines of evidence from earlier studies demonstrate that RNA helicase inhibitors are promising cancer drugs for the future (34, 35). Clearly, the diversity of DEAD/DEAH helicases in promoting cancer development warrants a broader evaluation of this protein family and the rational design of their inhibitors. Our study here demonstrates the importance of DHX33 in cell cycle transcriptional control and tumor development.

ACKNOWLEDGMENTS

We thank members of the Zhang lab for their technical input and suggestions and the staff in Department of Biology of the South University of Science and Technology of China (SUSTC) who provided support.

This work was supported by start-up funding from SUSTC (Y.Z.), by an SUSTC Basic Research Foundation (grant 22/Y01226024 to Y.Z.), and by the National Natural Science Foundation of China (31271550 to H.Z.).

We declare that we have no competing financial interests.

FUNDING INFORMATION

Southern University of Science and Technology of China provided funding under grant number 22/Y01226024 (Y. Zhang), and NSFC provided funding under grant number 31271550 (H. Zhong).

REFERENCES

1. **Fuller-Pace FV.** 1994. RNA helicases: modulators of RNA structure. Trends Cell Biol **4:**271–274. http://dx.doi.org/10.1016/0962-8924(94)90210-0.
2. **Linder P, Fuller-Pace FV.** 2013. The biology of RNA helicases-modulation for life. Preface. Biochim Biophys Acta **1829:**749. http://dx.doi.org/10.1016/j.bbagrm.2013.04.008.
3. **Zhang Y, Forys JT, Miceli AP, Gwinn AS, Weber JD.** 2011. Identification of DHX33 as a mediator of rRNA synthesis and cell growth. Mol Cell Biol **31:**4676–4691. http://dx.doi.org/10.1128/MCB.05832-11.
4. **Zhang Y, You J, Wang X, Weber J.** 2015 The DHX33 RNA helicase

promotes mRNA translation initiation. Mol Cell Biol **35:**2918–2931. http://dx.doi.org/10.1128/MCB.00315-15.

5. **Liu Y, Lu N, Yuan B, Weng L, Wang F, Liu YJ, Zhang Z.** 2014. The interaction between the helicase DHX33 and IPS-1 as a novel pathway to sense double-stranded RNA and RNA viruses in myeloid dendritic cells. Cell Mol Immunol **11:**49–57. http://dx.doi.org/10.1038/cmi.2013.40.
6. **Mitoma H, Hanabuchi S, Kim T, Bao M, Zhang Z, Sugimoto N, Liu YJ.** 2013. The DHX33 RNA helicase senses cytosolic RNA and activates the NLRP3 inflammasome. Immunity **39:**123–135. http://dx.doi.org/10.1016/j.immuni.2013.07.001.
7. **Zhang Y, Saporita AJ, Weber JD.** 2013. $p19^{ARF}$ and Ras^{V12} offer opposing regulation of DHX33 translation to dictate tumor cell fate. Mol Cell Biol **33:**1594–1607. http://dx.doi.org/10.1128/MCB.01220-12.
8. **Lemjabbar-Alaoui H, Hassan O, Yang YW, Buchanan P.** 2015. Lung cancer: biology and treatment options. Biochim Biophys Acta **1856:**189–210. http://dx.doi.org/10.1016/j.bbcan.2015.08.002.
9. **Cancer Genome Atlas Network.** 2014. Comprehensive molecular profiling of lung adenocarcinoma. Nature **511:**543–550. http://dx.doi.org/10.1038/nature13385.
10. **Govindan R, Ding L, Griffith M, Subramanian J, Dees ND, Kanchi KL, Maher CA, Fulton R, Fulton L, Wallis J, Chen K, Walker J, McDonald S, Bose R, Ornitz D, Xiong D, You M, Dooling DJ, Watson M, Mardis ER, Wilson RK.** 2012. Genomic landscape of non-small cell lung cancer in smokers and never-smokers. Cell **150:**1121–1134. http://dx.doi.org/10.1016/j.cell.2012.08.024.
11. **Takahashi T, Nau MM, Chiba I, Birrer MJ, Rosenberg RK, Vinocour M, Levitt M, Pass H, Gazdar AF, Minna JD.** 1989. p53: a frequent target for genetic abnormalities in lung cancer. Science **246:**491–494. http://dx.doi.org/10.1126/science.2554494.
12. **Kwak EL, Bang YJ, Camidge DR, Shaw AT, Solomon B, Maki RG, Ou SH, Dezube BJ, Jänne PA, Costa DB, Varella-Garcia M, Kim WH, Lynch TJ, Fidias P, Stubbs H, Engelman JA, Sequist LV, Tan W, Gandhi L, Mino-Kenudson M, Wei GC, Shreeve SM, Ratain MJ, Settleman J, Christensen JG, Haber DA, Wilner K, Salgia R, Shapiro GI, Clark JW, Iafrate AJ.** 2010. Anaplastic lymphoma kinase inhibition in non-small-cell lung cancer. N Engl J Med **363:**1693–1703. http://dx.doi.org/10.1056/NEJMoa1006448.
13. **Russo A, Franchina T, Ricciardi GR, Picone A, Ferraro G, Zanghi M, Toscano G, Giordano A, Adamo V.** 2015. A decade of EGFR inhibition in EGFR-mutated non small cell lung cancer (NSCLC): old successes and future perspectives. Oncotarget **6:**26814–26825. http://dx.doi.org/10.18632/oncotarget.4254.
14. **Scudellari M.** 2015. Drug development: mix and match. Nature **521:**S12–S14. http://dx.doi.org/10.1038/521S12a.
15. **Loupakis F, Pollina L, Stasi I, Ruzzo A, Scartozzi M, Santini D, Masi G, Graziano F, Cremolini C, Rulli E, Canestrari E, Funel N, Schiavon G, Petrini I, Magnani M, Tonini G, Campani D, Floriani I, Cascinu S, Falcone A.** 2009. PTEN expression and KRAS mutations on primary tumors and metastases in the prediction of benefit from cetuximab plus irinotecan for patients with metastatic colorectal cancer. J Clin Oncol **27:**2622–2629. http://dx.doi.org/10.1200/JCO.2008.20.2796.
16. **Westerfield M.** 2000. The zebrafish book: a guide for the laboratory use of zebrafish *Danio* (*Brachydanio*) *rerio*, 4th ed. University of Oregon Press, Eugene, OR.
17. **Kimmel CB, Ballard WW, Kimmel SR, Ullmann B, Schilling TF.** 1995. Stages of embryonic development of the zebrafish. Dev Dyn **203:**253–310. http://dx.doi.org/10.1002/aja.1002030302.
18. **Liu D, Wang Z, Xiao A, Zhang Y, Li W, Zu Y, Yao S, Lin S, Zhang B.** 2014. Efficient gene targeting in zebrafish mediated by a zebrafish-codon-optimized cas9 and evaluation of off-targeting effect. J Genet Genomics **41:**43–46. http://dx.doi.org/10.1016/j.jgg.2013.11.004.
19. **Chang N, Sun C, Gao L, Zhu D, Xu X, Zhu X, Xiong JW, Xi JJ.** 2013. Genome editing with RNA-guided Cas9 nuclease in zebrafish embryos. Cell Res **23:**465–472. http://dx.doi.org/10.1038/cr.2013.45.
20. **Qin W, Chen Z, Zhang Y, Yan R, Yan G, Li S, Zhong H, Lin S.** 2014 Jun 26. Nom1 mediates pancreas development by regulating ribosome biogenesis in zebrafish. PLoS One **9:**e100796.
21. **Calo E, Flynn RA, Martin L, Spitale RC, Chang HY, Wysocka J.** 2015. RNA helicase DDX21 coordinates transcription and ribosomal RNA processing. Nature **518:**249–253. http://dx.doi.org/10.1038/nature13923.
22. **Matallanas D, Crespo P.** 2010. New druggable targets in the Ras pathway? Curr Opin Mol Ther **12:**674–683.
23. **Downward J.** 2015. RAS synthetic lethal screens revisited: still seeking the elusive prize? Clin Cancer Res **21:**1802–1809. http://dx.doi.org/10.1158/1078-0432.CCR-14-2180.
24. **Morris EJ, Jha S, Restaino CR, Dayananth P, Zhu H, Cooper A, Carr D, Deng Y, Jin W, Black S, Long B, Liu J, Dinunzio E, Windsor W, Zhang R, Zhao S, Angagaw MH, Pinheiro EM, Desai J, Xiao L, Shipps G, Hruza A, Wang J, Kelly J, Paliwal S, Gao X, Babu BS, Zhu L, Daublain P, Zhang L, Lutterbach BA, Pelletier MR, Philippar U, Siliphaivanh P, Witter D, Kirschmeier P, Bishop WR, Hicklin D, Gilliland DG, Jayaraman L, Zawel L, Fawell S, Samatar AA.** 2013. Discovery of a novel ERK inhibitor with activity in models of acquired resistance to BRAF and MEK inhibitors. Cancer Discov **3:**742–750. http://dx.doi.org/10.1158/2159-8290.CD-13-0070.
25. **Linder P, Fuller-Pace FV.** 2013. Looking back on the birth of DEAD-box RNA helicases. Biochim Biophys Acta **1829:**750–755. http://dx.doi.org/10.1016/j.bbagrm.2013.03.007.
26. **Jarmoskaite I, Russell R.** 2014. RNA helicase proteins as chaperones and remodelers. Annu Rev Biochem **83:**697–725. http://dx.doi.org/10.1146/annurev-biochem-060713-035546.
27. **Botlagunta M, Vesuna F, Mironchik Y, Raman A, Lisok A, Winnard P, Jr, Mukadam S, Van Diest P, Chen JH, Farabaugh P, Patel AH, Raman V.** 2008. Oncogenic role of DDX3 in breast cancer biogenesis. Oncogene **27:**3912–3922. http://dx.doi.org/10.1038/onc.2008.33.
28. **Chen ZX, Wallis K, Fell SM, Sobrado VR, Hemmer MC, Ramskold D, Hellman U, Sandberg R, Kenchappa RS, Martinson T, Johnsen JI, Kogner P, Schlisio S.** 2014. RNA helicase A is a downstream mediator of KIF1Bβ tumor-suppressor function in neuroblastoma. Cancer Discov **4:**434–451. http://dx.doi.org/10.1158/2159-8290.CD-13-0362.
29. **Lin S, Tian L, Shen H, Gu Y, Li JL, Chen Z, Sun X, You MJ, Wu J.** 2013. DDX5 is a positive regulator of oncogenic NOTCH1 signaling in T cell acute lymphoblastic leukemia. Oncogene **32:**4845–4853. http://dx.doi.org/10.1038/onc.2012.482.
30. **Mazurek A, Luo W, Krasnitz A, Hicks J, Powers RS, Stillman B.** 2012. DDX5 regulates DNA replication and is required for cell proliferation in a subset of breast cancer cells. Cancer Discov **2:**812–825. http://dx.doi.org/10.1158/2159-8290.CD-12-0116.
31. **Mazurek A, Park Y, Miething C, Wilkinson JE, Gillis J, Lowe SW, Vakoc CR, Stillman B.** 2014. Acquired dependence of acute myeloid leukemia on the DEAD-box RNA helicase DDX5. Cell Rep **7:**1887–1899. http://dx.doi.org/10.1016/j.celrep.2014.05.019.
32. **Mills JR, Malina A, Lee T, Di Paola D, Larsson O, Miething C, Grosse F, Tang H, Zannis-Hadjopoulos M, Lowe SW, Pelletier JRN.** 2013. Ai screening uncovers Dhx9 as a modifier of ABT-737 resistance in an Emu-myc/Bcl-2 mouse model. Blood **121:**3402–3412. http://dx.doi.org/10.1182/blood-2012-06-434365.
33. **Parsyan A, Shahbazian D, Martineau Y, Petroulakis E, Alain T, Larsson O, Mathonnet G, Tettweiler G, Hellen CU, Pestova TV, Svitkin YV, Sonenberg N.** 2009. The helicase protein DHX29 promotes translation initiation, cell proliferation, and tumorigenesis. Proc Natl Acad Sci U S A **106:**22217–22222. http://dx.doi.org/10.1073/pnas.0909773106.
34. **Bol GM, Vesuna F, Xie M, Zeng J, Aziz K, Gandhi N, Levine A, Irving A, Korz D, Tantravedi S, Heerma van Voss MR, Gabrielson K, Bordt EA, Polster BM, Cope L, van der Groep P, Kondaskar A, Rudek MA, Hosmane RS, van der Wall E, van Diest PJ, Tran PT, Raman V.** 2015. Targeting DDX3 with a small molecule inhibitor for lung cancer therapy. EMBO Mol Med **7:**648–669. http://dx.doi.org/10.15252/emmm.201404368.
35. **Samal SK, Routray S, Veeramachaneni GK, Dash R, Botlagunta M.** 2015. Ketorolac salt is a newly discovered DDX3 inhibitor to treat oral cancer. Sci Rep **5:**9982. http://dx.doi.org/10.1038/srep09982.
36. **Rhodes DR, Yu J, Shanker K, Deshpande N, Varambally R, Ghosh D, Barrette T, Pandey A, Chinnaiyan AM.** 2004. ONCOMINE: a cancer microarray database and integrated data-mining platform. Neoplasia **6:**1–6. http://dx.doi.org/10.1016/S1476-5586(04)80047-2.